agriculture

MDPI

Article

Spatio-Temporal Variation and Future Sustainability of Net Primary Productivity from 2001 to 2021 in Hetao Irrigation District, Inner Mongolia

Manman Peng [1,2], Chaoqun Li [1,2,*], Peng Wang [3,4] and Xincong Dai [5]

[1] College of Mechanical and Electrical Engineering, Heze University, Heze 274015, China; tina0808@nwafu.edu.cn
[2] College of Mechanical and Electronic Engineering, Northwest A&F University, Yangling 712100, China
[3] College of Mechanical and Electrical Engineering, Shanxi Datong University, Datong 037003, China; wangpeng1994@hnu.edu.cn
[4] College of Mechanical and Vehicle Engineering, Hunan University, Changsha 410082, China
[5] School of Computer Science, Northwestern Polytechnical University, Xi'an 710129, China; pooh@mail.nwpu.edu.cn
* Correspondence: chaoqun92@nwafu.edu.cn; Tel.: +86-15557361938

Abstract: The Hetao Irrigation District in Inner Mongolia, a vital grain-producing region in northern China, faces growing environmental challenges. Studying net primary productivity (NPP) is essential for understanding spatiotemporal vegetation shifts and guiding locally adapted restoration and management efforts. Utilizing MOD17A3/NPP data, this study applies the Theil–Sen median trend, Mann–Kendall significance, and the Hurst index to scrutinize the spatiotemporal distribution patterns of NPP from 2001 to 2021 and forecast future changes in the area. The findings reveal cyclic temporal trends, forming a "∧" shape with initial increases followed by decreases, notably during the July to August period each year. The multi-year average NPP exhibits a slight upward fluctuation trend, averaging 172.40 $gCm^{-2}a^{-1}$. Peaks occur approximately every three years, reaching the highest average in 2012 at 218.96 $gCm^{-2}a^{-1}$. Spatially, NPP distribution stays consistent over the years, influenced by various land cover types, especially cropland, shaping the spatial patterns. Monthly and yearly NPP trends over the 21 years indicate a significant decrease in May and June, with other months mostly showing a non-significant increase. The Hurst index for monthly and yearly NPP changes over 21 years shows relatively high weak anti-persistence. In summary, over the past 21 years, the NPP trend in the study area has not significantly improved and is expected to decline in the future. This study offers data support and a scientific foundation for refining the carbon cycle model, quantifying vegetation carbon sequestration capacity, addressing climate change policies, and striving for carbon peak and neutrality in the Hetao Irrigation District.

Keywords: net primary productivity; Hetao Irrigation District; spatial and temporal patterns; Hurst index; carbon peak and carbon neutrality

Citation: Peng, M.; Li, C.; Wang, P.; Dai, X. Spatio-Temporal Variation and Future Sustainability of Net Primary Productivity from 2001 to 2021 in Hetao Irrigation District, Inner Mongolia. *Agriculture* **2024**, *14*, 613. https://doi.org/10.3390/agriculture14040613

Academic Editor: Josef Eitzinger

Received: 2 March 2024
Revised: 2 April 2024
Accepted: 10 April 2024
Published: 15 April 2024

1. Introduction

Land ecosystems, serving as crucial carbon reservoirs in the global carbon cycle, exert profound impacts on the carbon cycle at a global scale [1,2]. Vegetation, as the core component of terrestrial ecosystems, plays a critical role in reducing greenhouse gas concentrations, maintaining global material and energy cycles, and preserving the global carbon balance. NPP refers to the amount of organic matter accumulated by green plants through photosynthesis per unit time and unit area, excluding the amount consumed by their own respiration [3]. NPP is a key link in ecosystem carbon cycling and energy flow, directly or indirectly reflecting the carbon potential of regional ecosystems. The spatiotemporal distribution characteristics of NPP have become crucial for understanding

the regional vegetation growth status, CO_2 uptake capacity, assessing ecosystem functions, and effectively reflecting the quality of land cover and ecosystems [4,5]. NPP in terrestrial ecosystems displays notable spatial heterogeneity. In the pursuit of the "carbon peak" and "carbon neutrality" goals, discerning the differences and changes in NPP at temporal and spatial scales holds great significance for the evolution of terrestrial ecosystems and the adjustment of the carbon balance.

Currently, both domestic and international estimates of NPP in terrestrial ecosystems primarily utilize two main approaches: the "bottom-up" and "top-down" methods. Initially, the "bottom-up" method involved setting fixed ranges as study areas and acquiring NPP through continuous observation and surveys [6–9]. For example, widely used in agricultural greenhouse gas flux studies, the chamber method system has been extensively applied [10]. In previous studies, improvements were made to the commonly used chamber method system, successfully applied in field experiments, and yielding certain results (e.g., [10–13]). However, challenges persist in meeting regional-scale demands. With advancements in field observation techniques, the eddy covariance system is primarily used at the regional scale [9,14]. However, the mobility of the eddy covariance system is limited, making it difficult to comprehensively observe various ecological types within the same region. Additionally, issues such as long sampling periods and incomplete coverage persist [15,16]. In summary, although traditional NPP measurement and observation methods provide precise NPP data, their destructive impact on vegetation, coupled with cost constraints, poses significant implementation challenges, thereby failing to meet researchers' demands for long-term and regional-scale monitoring.

With the continuous development of remote sensing technology, remote sensing images are widely used in various research fields to acquire high spatiotemporal surface information [13]. Satellite remote sensing can overcome the limitations of ground-based single-point measurements, helping to expand observations from fixed points to regional scales [17]. Remote sensing data, characterized by long time series and wide coverage, has become an essential means for estimating the spatiotemporal characteristics and driving mechanisms of global vegetation NPP through top-down research methods based on remote sensing data inversion [17]. Currently, both domestically and internationally, the monitoring of large-scale vegetation NPP relies mainly on remote sensing interpretation estimates [18]. MODIS data, due to its high temporal resolution and low cost, has become one of the primary remote sensing data sources for simulating and estimating regional vegetation NPP [19]. MODIS products use the process-based Biome-BGC ecological model for NPP estimation. Compared with traditional regression models, the Biome-BGC process model employs more parameters and more sophisticated estimation methods, improving the accuracy of NPP estimation [20]. In recent years, MOD17A3 data products have been widely validated and applied in global and regional carbon cycle research [21]. Many scholars have used the Google Earth Engine (GEE) platform or the platform provided by the National Aeronautics and Space Administration (NASA) to access MODIS datasets, studying the correlations between NPP and various factors at different scales. They have verified the impacts of factors such as precipitation, land cover changes, temperature, and human activities on NPP, enhancing our understanding of and insights into vegetation NPP in specific regions of China [19,22,23]. However, the factors influencing NPP vary across different regions and time periods. The formation of vegetation NPP is a complex process influenced by multiple factors, involving disciplines such as plant physiology, hydrology, meteorology, soil science, physics, and disaster research. Terrestrial ecosystems are the dynamic products of interactions between natural and human factors [21]. Current research often focuses only on single or limited factors affecting vegetation NPP. Future research should pay more attention to the synergistic effects of multiple factors, thoroughly analyzing the complex mechanisms underlying vegetation NPP formation, to comprehensively explore the dynamic evolution of terrestrial ecosystems and the adjustment of carbon balance. In-depth analysis of vegetation NPP at different spatial and temporal scales in the

study area has become a prerequisite for exploring the complex mechanisms underlying vegetation NPP formation.

The Hetao Irrigation District in Inner Mongolia, located in arid and semi-arid regions of China, serves as a crucial commodity grain base in northern China and stands as a typical artificial agricultural oasis. With the rapid development of oasis agriculture, the pressure on the ecological environment in this region continues to increase, and various environmental issues are gradually becoming prominent, making it a sensitive area for sustainable development in northern China [24,25]. By analyzing the spatial distribution characteristics and temporal changes of NPP in the Hetao Irrigation District of Inner Mongolia, we can understand the variations in organic matter accumulation in vegetation in recent years. This contributes to maintaining the carbon cycle of the ecosystem in the Hetao Irrigation District, building ecological barriers, and providing references for ecological environmental management and sustainable development in the Hetao Irrigation District. Currently, most studies on NPP in Inner Mongolia focus on analyzing the annual spatiotemporal distribution of NPP, without delving into monthly or 8-day temporal variations. Moreover, these studies primarily emphasize the analysis of the response of NPP to individual factors such as temperature and precipitation (e.g., [21,26–28]). Focusing solely on the analysis of the response of vegetation NPP to individual factors while neglecting the spatial variability analysis of NPP across multiple temporal and spatial scales is insufficient for understanding the current carbon cycling capacity of regional ecosystems and future development trends.

Therefore, this study is based on vegetation NPP data extracted from MOD17A3/NPP data products for the Hetao Irrigation District of Inner Mongolia from 2001 to 2021, aiming to analyze its spatiotemporal evolution characteristics. The specific research objectives include: (1) Analyzing the spatiotemporal variation characteristics of NPP in the Hetao Irrigation District of Inner Mongolia from 2001 to 2021 at different temporal scales; (2) Utilizing Theil–Sen Median trend analysis and Mann–Kendall test methods to analyze the changing trends of NPP in the Hetao Irrigation District of Inner Mongolia for the past 21 years (2001–2021) at the pixel level; (3) Finally, analyzing the future trends of vegetation NPP in the study area through Hurst index analysis. The research results are of great significance for evaluating the carrying capacity of the ecosystem in the Hetao Irrigation District of Inner Mongolia and formulating sustainable development policies.

2. Data and Research Methods

2.1. Study Area

The Hetao Irrigation District is located in the western part of the Inner Mongolia Autonomous Region (40°–41° N, 107°–109° E), spanning seven banners, counties, districts, and a small part of the suburbs of Baotou City. It stretches approximately 300 km from east to west and is 50 to 80 km wide from north to south, with a total land area of about 11,600 square kilometers (Figure 1). It is a super-large irrigation area in the upstream area of the Yellow River and a typical representative of the largest self-flowing irrigation system in Asia. The climate of the region belongs to a typical temperate continental climate, with an average annual temperature ranging from 6.3 to 7.7 °C. Due to its location in the arid and semi-arid regions of northwestern inland, the average annual rainfall and evaporation amount to 160 mm and 2240 mm, respectively, making the Yellow River irrigation a necessary condition for agricultural production in the area. The terrain of the Hetao Irrigation District is flat, with predominant soil types including salinized alluvial soil, saline soil, and tidal alluvial soil. The soil texture mainly consists of loamy soil, sandy loam, fine clay, and a small amount of fine sandy soil. The soil layer is deep, belonging to lacustrine sedimentary plains [24,29,30]. The entire irrigation area is primarily agricultural, with cultivated land accounting for approximately 47% of the total area and grassland accounting for about 23% (Figure 1a).

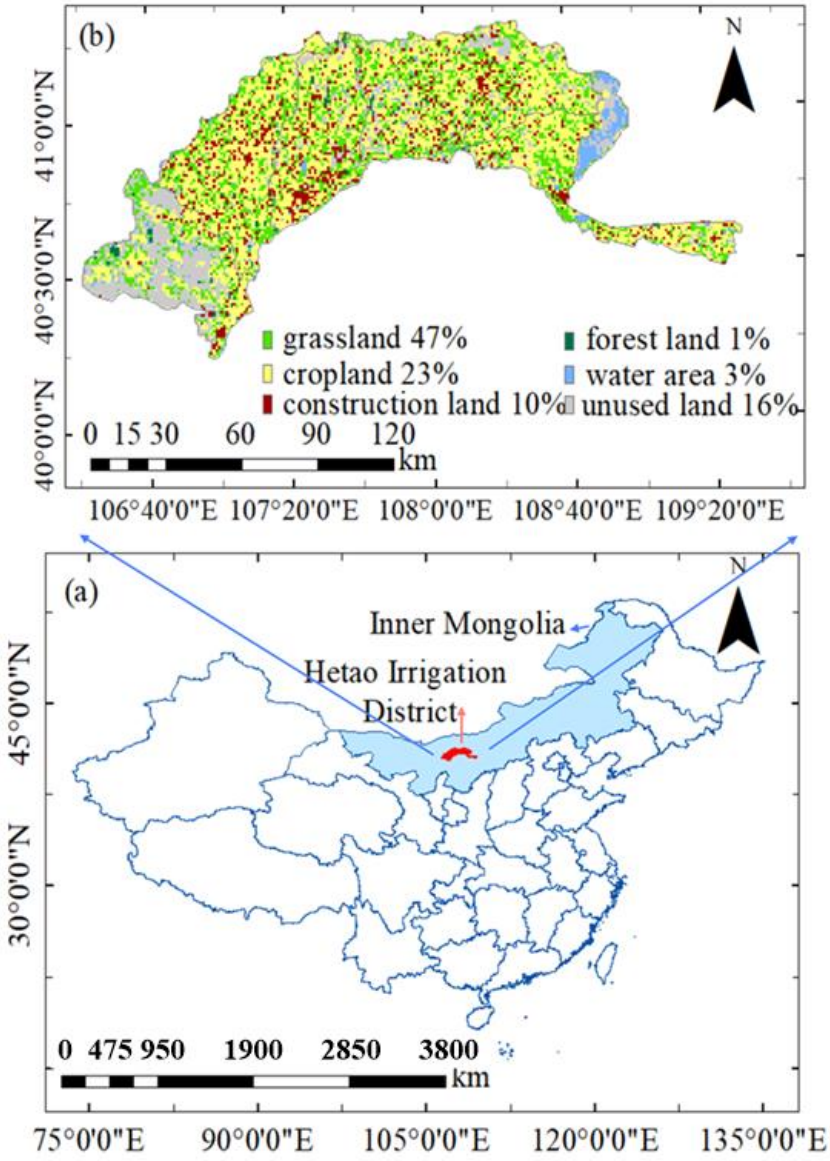

Figure 1. Location of the study area. (**a**) Map of China with highlighted study area; (**b**) land use spatial distribution map of study area.

2.2. Data Sources

NPP data are obtained from the Earth Engine Data Catalog "https://developers.google.com/earth-engine/datasets/catalog/?filter=MODIS/006/MOD17A3HGF (10 November 2023)", which, to a certain extent, addresses data attenuation and distortion issues caused by aging satellite sensors [23,31]. As the current globally widespread dataset with the longest time span, well-defined physiological and ecological mechanisms, and accurate estimation results for land vegetation NPP, this dataset is one of the most extensively used sources in global and regional studies of vegetation NPP and carbon cycling, receiving widespread applications. In this study, we selected vegetation NPP data from 2001 to 2021, with a spatial resolution of 500 m, a temporal resolution of one year, and the unit of measurement as kgC/m^2, utilizing a sinusoidal projection. The retrieval of NPP data is executed through code implemented within the GEE, involving processes such as data mosaicking, reprojection, format conversion, clipping, and unit conversion. The final dataset for the Hetao Irrigation District is obtained in units of gC/m^2.

2.3. Methods

2.3.1. Theil–Sen Median Trend Analysis and Mann–Kendall Test

The Theil–Sen Median method, also known as Sen's slope estimator, is a robust non-parametric statistical method used for trend estimation. This method is computationally efficient and insensitive to measurement errors and outliers, making it particularly suitable for trend analysis of long time series data [32,33]. Sen's slope estimator is widely used for calculating trend values and is commonly combined with the Mann–Kendall (MK) non-parametric test method. The Mann–Kendall test is a non-parametric method for testing the trend in time series data. Its advantages include not requiring the measured values to follow a normal distribution and not assuming that the trend is linear. Additionally, the Mann–Kendall test is robust to missing values and outliers, making it widely used for trend significance testing in long time series data [34]. The formula for calculating Sen's slope (β) is:

$$\beta = Median\left(\frac{x_j - x_i}{j - i}\right), \forall_j > i \tag{1}$$

where *Median ()* represents taking the median. When $\beta > 0$, it indicates a growing trend in vegetation NPP; if $\beta = 0$, it suggests no significant change in vegetation NPP; and when $\beta < 0$, it indicates a decreasing trend in vegetation NPP. x_j and x_i represent the values of NPP in the time series for the j and i years or months, respectively.

The calculation steps for the Mann–Kendall (MK) significance test are as follows:

$$S = \sum_{i=1}^{n-1} \sum_{j=i+1}^{n} sgn(x_j - x_i) \tag{2}$$

$$Z = \begin{cases} \frac{S}{\sqrt{Var(S)}} & (S > 0) \\ 0 & (S = 0) \\ \frac{S+1}{\sqrt{Var(S)}} & (S < 0) \end{cases} \tag{3}$$

$$Var(S) = \frac{n(n-1)(2n+5)}{18} \tag{4}$$

where x_i and x_j represent the values of x and y in the i and j years, respectively, and n is the total number of data points. Z is the standardized test statistic. This method assesses the significance of the time series trend by calculating Z. The standardized Z values follow a standard normal distribution, and based on the confidence level of 95%, the corresponding values from the standard normal distribution table are used. In other words, the region where $|Z| > 1.96$ indicates a significant trend, while the opposite suggests an insignificant trend. The determination of trend significance is outlined in Table 1. Based on the results of Sen trend analysis and the MK test, this study categorizes the trend changes in NPP in the Hetao Irrigation District from 2001 to 2021 into seven categories according to the criteria in Table 1.

Table 1. Mann–Kendall test for trend categories.

β	Z	Trend Type	Trend Features
$\beta > 0$	$2.58 < Z$	4	extremely significant increase
	$1.96 < Z \leq 2.58$	3	significant increase
	$1.65 < Z \leq 1.96$	2	slightly significant increase
	$Z \leq 1.65$	1	no significant increase
$\beta = 0$	Z	0	no change
$\beta < 0$	$Z \leq 1.65$	−1	no significant decrease
	$1.65 < Z \leq 1.96$	−2	slightly significant decrease
	$1.96 < Z \leq 2.58$	−3	significant decrease
	$2.58 < Z$	−4	extremely significant decrease

2.3.2. The Hurst Index

The Hurst index is a method used to assess long-term dependence in time series data, and it can be calculated using the R/S analysis method [35]. In this study, the Hurst index is utilized to assess the sustainability of vegetation NPP changes in the Hetao Irrigation District of Inner Mongolia and predict future trends. The specific calculation formulas and steps are as follows:

Define the time series of vegetation *NPP* variation in the Hetao Irrigation District of Inner Mongolia:

$$NPP_t = \frac{1}{\tau}\sum_{t=1}^{\tau} NPP_t, \tau = 1, 2, 3, \cdots, n \quad (5)$$

Calculate cumulative deviation:

$$X_{(t,\tau)} = \sum_{t=1}^{\tau} \left(NPP_t - \overline{NPP_\tau}\right), 1 \le t \le \tau \quad (6)$$

Calculate the range of the time series:

$$R_\tau = maxX_{(t,\tau)} - minX_{(t,\tau)}, 1 \le t \le \tau, \tau = 1, 2, 3, \cdots, n \quad (7)$$

Calculate the standard deviation:

$$S_\tau = \left[\frac{1}{\tau}\sum_{t=1}^{\tau} \left(NPP_t - \overline{NPP_\tau}\right)^2\right]^{1/2}, \tau = 1, 2, 3, \cdots, n \quad (8)$$

Fit the Hurst index exponent:

$$\frac{R_\tau}{S_\tau} = (C\tau)^H \quad (9)$$

The Hurst index, denoted as Hurst $\in$ (0, 1), signifies different characteristics of the NPP time series changes. When Hurst = 0.5, it indicates a random pattern with no long-term correlation. For 0 < Hurst < 0.5, the NPP time series exhibits anti-persistence, with a stronger anti-persistence as Hurst approaches 0. When 0.5 < Hurst < 1, it suggests a persistent and long-term correlated NPP series, where a higher Hurst index closer to 1 indicates stronger time series persistence, implying consistency in future trends with the past.

3. Results and Analysis

3.1. Analysis of Temporal Changes in NPP at Different Scales

The temporal variations in NPP in the Hetao Irrigation District of Inner Mongolia from 2001 to 2021 are depicted in Figures 2–4. The overall trends on an 8-day and monthly basis exhibit a periodic "∧"-shaped pattern with peaks typically occurring at the end of July or beginning of August every year, NPP values remain close to 0 from late October to early March of the following year (Figures 2 and 3). Peng et al. [10] researching in the Hetao Irrigation District of Inner Mongolia found that vegetation experiences its peak growth, and photosynthetic capacity is at its strongest around July each year. Studies by Zhang et al. [36] have indicated that young vegetation in agricultural ecosystems demonstrates limited carbon assimilation capacity. Moreover, research by Wang et al. [37] suggests that plants require more carbon for growth, canopy development, and grain filling around July each year, explaining the observed high NPP values during this period. Xi et al. [38] found that during the maturation phase, both photosynthesis and respiration intensity in crops significantly decreases, elucidating the observed pattern of increasing NPP followed by a decrease within a year.

The 8-day variation of the Hetao Irrigation District in Inner Mongolia from 2001 to 2021 reveals outliers in August of both 2019 and 2021 (Figure 2a), which may be attributed to data attenuation and distortion caused by weather conditions or aging of satellite sensors [39]. The mean NPP value in July 2018 reached its maximum at 17.726 gCm^{-2} (Figure 2b). It

is noteworthy that the NPP changes observed every 8 days exhibit a serrated "∧"-shaped fluctuation, primarily due to short-term variations influenced by factors such as weather and solar radiation intensity [10–12,40]. However, the monthly variation of NPP in the Hetao Irrigation District of Inner Mongolia from 2001 to 2021 shows a relatively smooth curve, with peak values occurring in July or August each year (Figure 3a). The maximum monthly mean NPP appeared in August 2012, with a value of 15.52 gCm^{-2} (Figure 3b). Figure 4 shows a slight upward fluctuation trend in NPP in the Hetao Irrigation District of Inner Mongolia from 2001 to 2021, with annual averages ranging between 132.40 and 218.96 $gCm^{-2}a^{-1}$. The average NPP over 21 years is 172.40 $gCm^{-2}a^{-1}$, consistent with the annual average NPP reported in previous studies conducted in Inner Mongolia [21,26–28]. Peaks in NPP occur approximately every 3 years, notably in 2004, 2008, 2012, 2016, and 2019, with the maximum recorded in 2012 (218.96 $gCm^{-2}a^{-1}$) and the minimum in 2001 (132.40 $gCm^{-2}a^{-1}$) (Figure 4b). The fluctuations in annual NPP are primarily influenced by both human and natural factors [21,41]. For instance, the relatively lower NPP observed in 2017 compared to the preceding and succeeding years may be attributed to an extreme drought event occurring that year. In arid and semi-arid regions, precipitation is one of the primary factors influencing NPP variability [42]. Previous studies have reported a greater reduction in NPP due to water stress than observed in this study [43,44]. Plants in long-term water-stressed areas exhibit extremely high water-use efficiency, making them highly resistant to short-term droughts [45]. However, even with a slight increase in water stress, NPP does not significantly decrease. Significant impacts on vegetation growth and photosynthesis inhibition occur only when water stress reaches higher levels in these regions [46–48], consistent with the findings of Hao et al. [26] in Inner Mongolia.

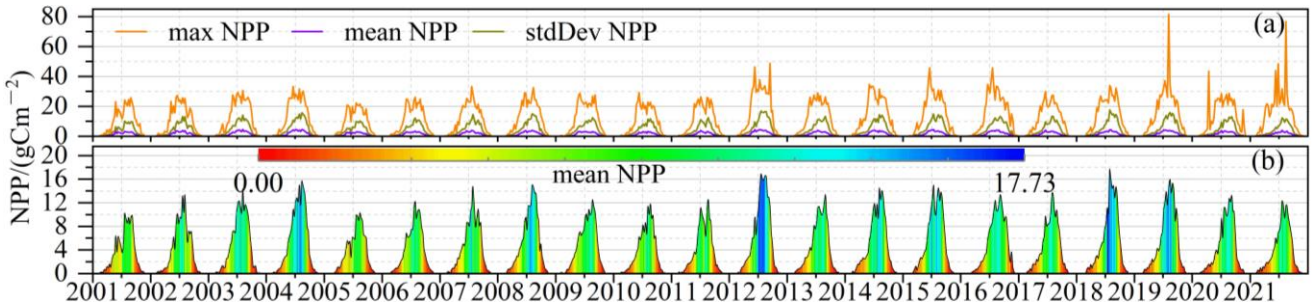

Figure 2. NPP changes every 8 days from 2001 to 2021. (**a**) The max, mean, and stdDev of NPP in the study area; (**b**) The mean value of NPP in the study area.

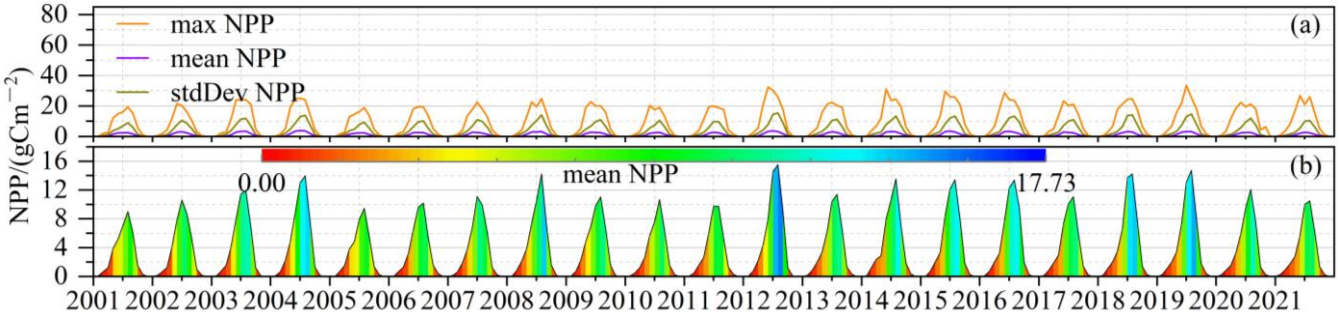

Figure 3. Monthly NPP changes from 2001 to 2021. (**a**) The max, mean, and stdDev of NPP in the study area; (**b**) The mean value of NPP in the study area.

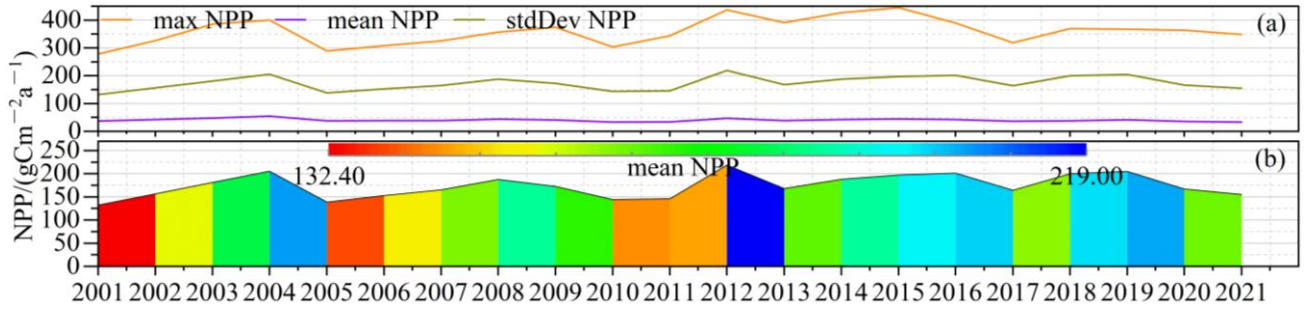

Figure 4. Annual NPP changes from 2001 to 2021. (**a**) The max, mean, and stdDev of NPP in the study area; (**b**) The mean value of NPP in the study area.

3.2. Analysis of Spatial Variation of NPP at Different Scales

Spatial and temporal variations of NPP (gCm^{-2}a^{-1}) in the study area from 2001 to 2021 are depicted in Figure 5. From the graph, it can be observed that the spatial distribution of NPP changes consistently over the years, with NPP values ranging from small (indicated in red) to large (indicated in blue). Typically, construction land and unused land exhibit red color in the annual variation, indicating minimal NPP values, and show little change over the years. Meanwhile, larger NPP values are predominantly distributed in cropland and grassland where green vegetation growth occurs, represented by green color. Taking the land use in the Hetao Irrigation District in 2021 as an example, the predominant land use is cropland, accounting for 47% of the total area, followed by grassland at 23%, with forestland occupying only 1%. This disparity in land cover composition is the primary driver of spatial variations in NPP. Previous studies [22,26] have also demonstrated the significant contribution of cropland to NPP.

Using the example of the year 2021, Figure 6 illustrates the monthly spatiotemporal changes in NPP within the study area. NPP changing from red to blue and back to red over the course of a year indicates a transition from low to high and back to low NPP values. Typically, NPP reaches its maximum in July or August, when vegetation growth is at its peak [10,13]. In January, February, November, and December, the map appears deep red, so NPP is relatively low during the course of the year. This is because in these months, the Hetao Irrigation District is covered by snow, and the soil is in a frozen state, resulting in minimal green vegetation growth and the lowest NPP values [49]. Starting from March, as the frozen soil layer gradually melts, NPP across the entire basin begins to increase, primarily driven by forest and grassland areas. By the end of May and early June, crops in the Hetao Irrigation District have been sown [10,13,40]. In June, as the crops germinate and grow, NPP gradually rises. However, since the crops are still small at this point, with relatively small leaf areas for photosynthesis, the overall NPP remains relatively low. July and August represent the peak growing period for crops. For example, during this time, maize in the Hetao Irrigation District is in the tassel stage, and sunflowers are in the budding stage [50]. Crops exhibit their maximum photosynthetic capacity during this period, resulting in the peak of NPP. In September, as crops mature, leaves gradually turn yellow, and the green leaf area decreases, leading to a gradual decline in NPP. This decline continues until the end of September and October, when crop harvesting is completed, and NPP across the entire region gradually decreases to its minimum.

3.3. Spatial–Temporal Distributions and Variations of NPP Trend

The Sen + Mann–Kendall algorithm was employed to analyze the monthly and interannual variations of NPP over the 21-year study period. Figures 7 and 8 depict the corresponding outcomes. Table 2 provides a detailed account of the area and proportion of different trend changes within the study area. It is noteworthy that the gray areas in the table represent unused land where NPP remained unchanged, primarily because these regions were not considered during the data analysis process. Additionally, data gaps were observed in the images for January, February, and December.

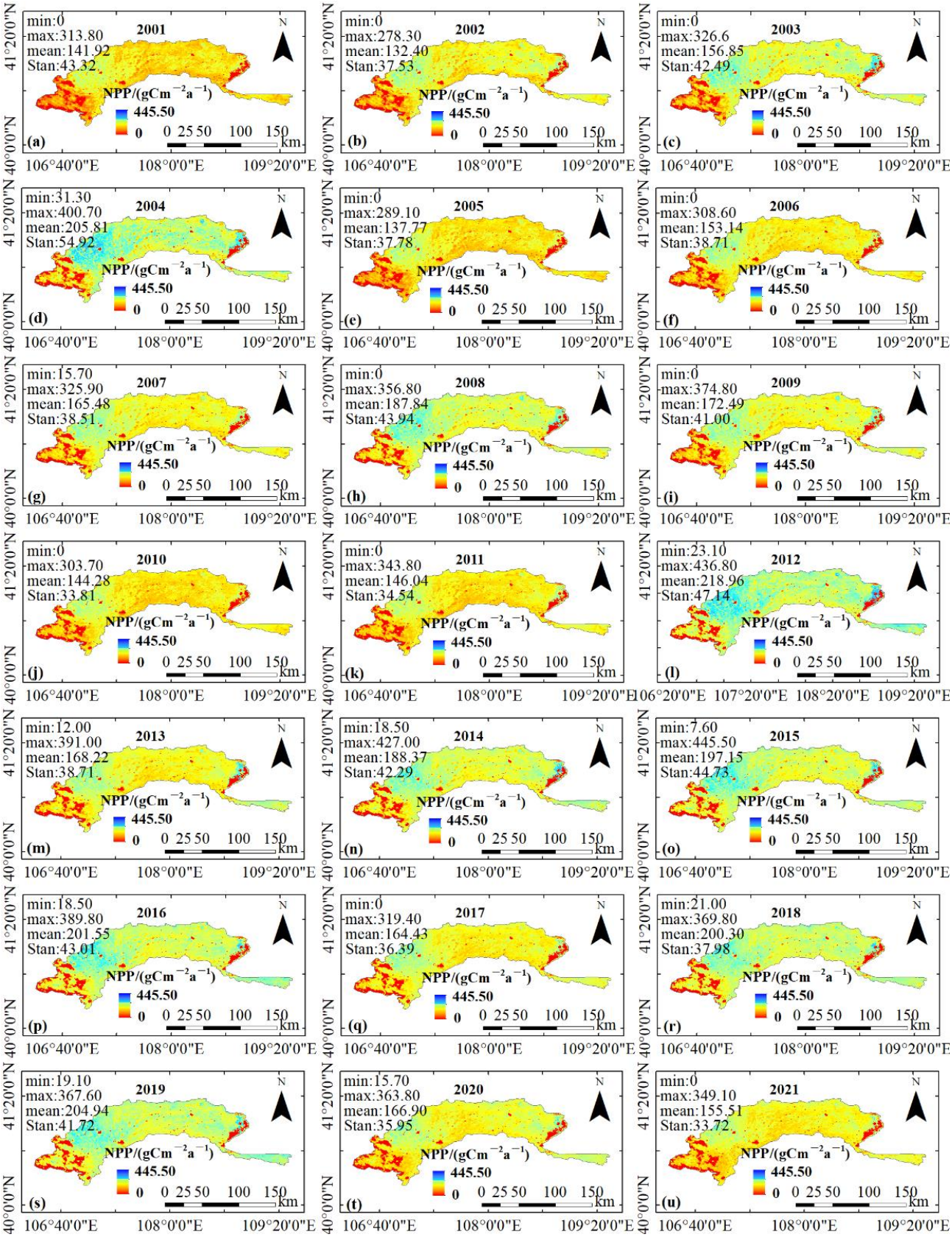

Figure 5. The spatiotemporal variation of annual NPP from 2001 to 2021. (**a**) 2001; (**b**) 2002; (**c**) 2003; (**d**) 2004; (**e**) 2005; (**f**) 2006; (**g**) 2007; (**h**) 2008; (**i**) 2009; (**j**) 2010; (**k**) 2011; (**l**) 2012; (**m**) 2013; (**n**) 2014; (**o**) 2015; (**p**) 2016; (**q**) 2017; (**r**) 2018; (**s**) 2019; (**t**) 2020; (**u**) 2021.

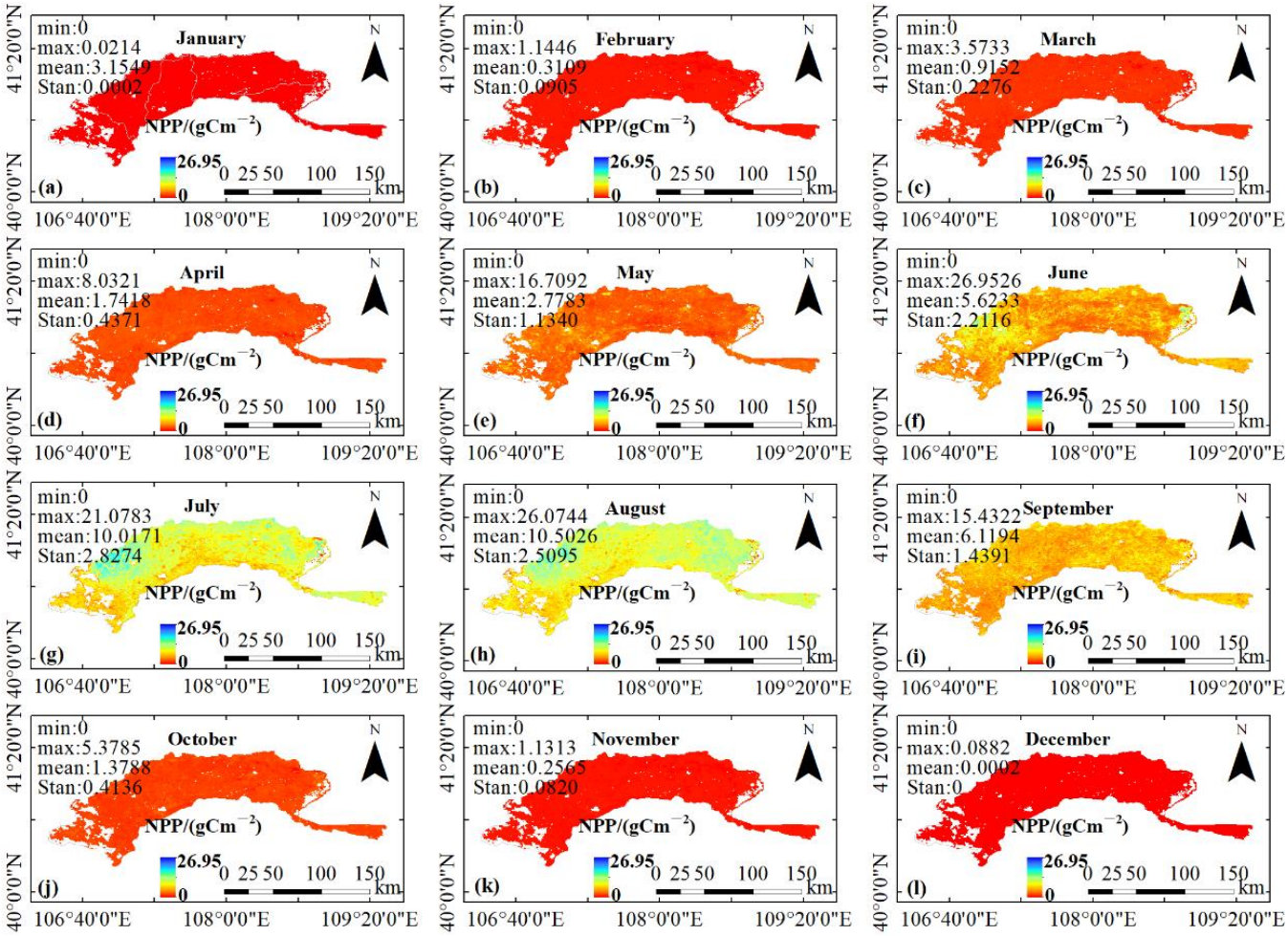

Figure 6. The spatiotemporal variation of monthly NPP in 2021. (**a**) January; (**b**) February; (**c**) March; (**d**) April; (**e**) May; (**f**) June; (**g**) July; (**h**) August; (**i**) September; (**j**) October; (**k**) November; (**l**) December.

Overall, from 2001 to 2021, the vegetation NPP in the Hetao Irrigation District exhibited spatial heterogeneity in its changing trends. Specifically, for the months from February to November and the entire year, the proportions of positively changing trends (trend category > 0) were as follows: 70.28%, 89.44%, 81.98%, 19.73%, 47.09%, 82.38%, 89.72%, 83.47%, 70.80%, 79.18%, and 86.12%, respectively. On the other hand, the proportions of negatively changing trends (trend category < 0) were: 0.07%, 1.97%, 10.32%, 72.79%, 45.44%, 10.14%, 2.82%, 9.06%, 21.44%, 5.51%, and 6.34%, respectively. The results indicate that over the past 21 years, the positive proportions of NPP variation from February to November and annual changes have been significant. From the bar graph illustrating the proportions of different trend changes across the study area in Table 2, it is evident that the proportion of positive changes is significantly larger, with a notable percentage falling under the category of insignificant increase. It is noteworthy that negative trends appear in May and June, primarily characterized by significant and extremely significant decreases, with May exhibiting the highest proportion of extremely significant decrease, reaching 33.86% (Figure 9). This trend mainly occurs in agricultural areas, and is attributed to the months-long thawing of permafrost in Inner Mongolia, leading to soil tillage for crop seeding, which increases soil respiration [51], releasing significant amounts of CO_2, and consequently reducing NPP. Additionally, during the early stages of crop growth, the smaller leaf area leads to lower photosynthetic capacity, resulting in lower NPP [10,13,40]. As time progresses, by June, the photosynthetic capacity of crops gradually increases, enhancing their ability for CO_2 uptake, thereby promoting an increase in NPP. Since 2000, various ecological compensation measures have been implemented to address land

degradation issues in Inner Mongolia, including direct economic compensation for fallow land, grazing bans on grasslands, and afforestation and grassland restoration projects [52,53]. These measures have led to a reduction in arable land in the Hetao Irrigation District. Consequently, the significant decrease in NPP in May has become a dominant trend over the past 21 years.

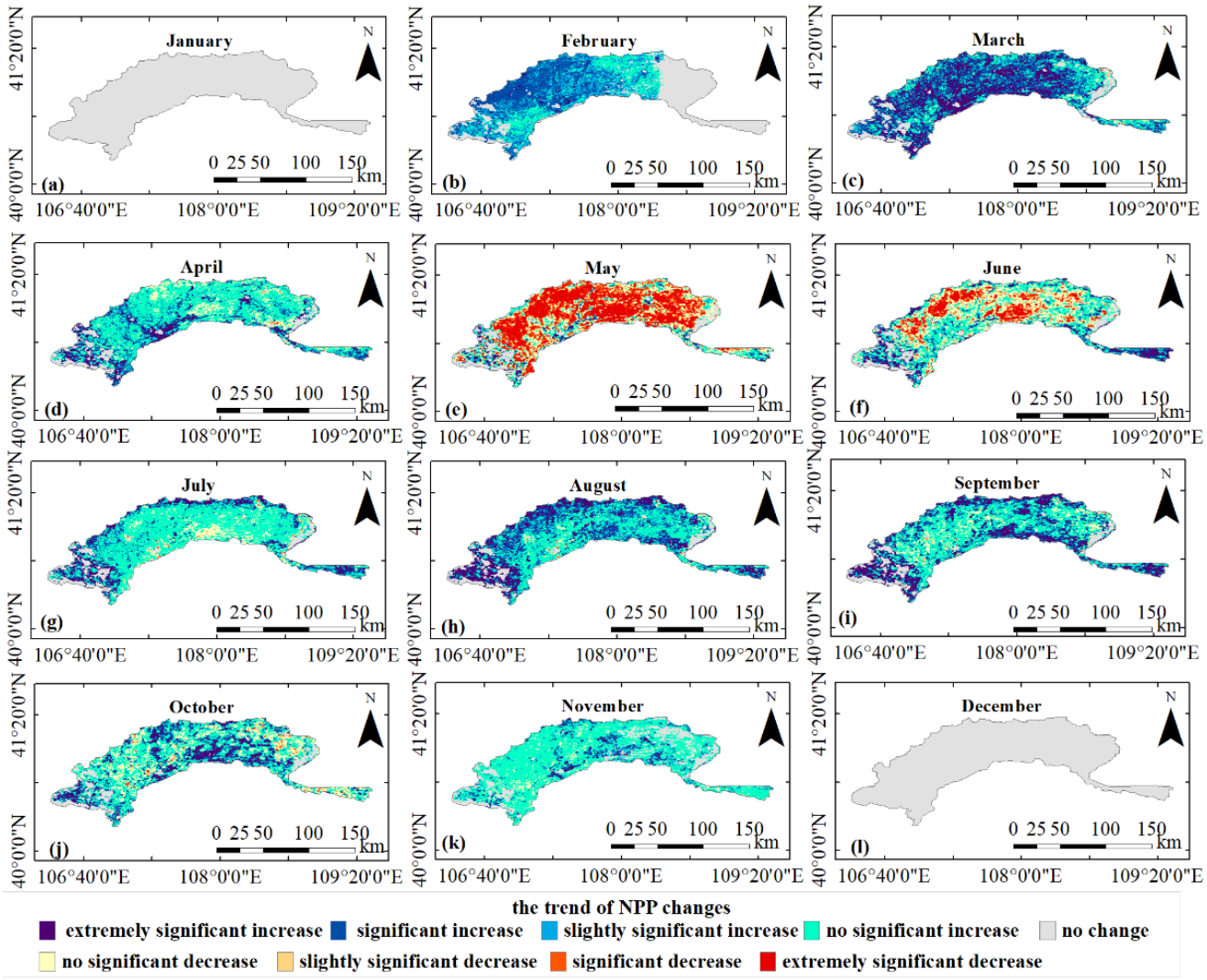

Figure 7. Distribution of monthly NPP changes from 2001 to 2021 based on the Sen + Mann algorithm. (**a**) January; (**b**) February; (**c**) March; (**d**) April; (**e**) May; (**f**) June; (**g**) July; (**h**) August; (**i**) September; (**j**) October; (**k**) November; (**l**) December.

In terms of interannual changes, the NPP trend in the study area still exhibits spatial heterogeneity, with positive changes (trend category > 0) occupying 86.16% of the total area. However, this positive change mainly manifests as an insignificant increase, covering 51.00% of the total area. In contrast, the area proportion of negative changes (trend category < 0) is only 6.34%. This further indicates that over the past 21 years, there has been a tendency for an increase in vegetation NPP in the Hetao Irrigation District of Inner Mongolia. However, the overall increase is not significant, suggesting that the carbon cycling process in the ecosystem of the study area has not significantly improved over the past 21 years. Relevant policies need to be implemented to construct ecological barriers and achieve ecological environmental management and sustainable development in the Hetao Irrigation District.

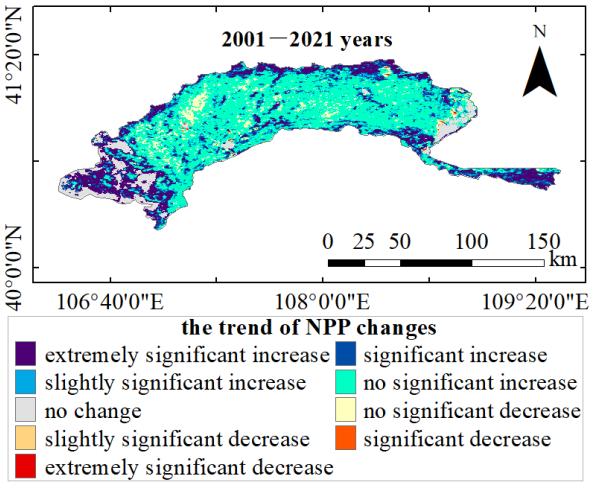

Figure 8. Distribution of annual NPP changes from 2001 to 2021 based on the Sen + Mann algorithm.

Table 2. Area and proportion of NPP changes at different levels based on Sen + Mann from 2001 to 2021.

Time	Parameter	NPP Change Trend Categories								
		4	**3**	**2**	**1**	**0**	**−1**	**−2**	**−3**	**−4**
1/January	Area	-	-	-	-	-	-	-	-	-
	ArO	-	-	-	-	-	-	-	-	-
2/February	Area	0.85	31.82	26.62	21.21	34.04	0.08	0	-	-
	ArO	0.74	27.78	23.24	18.52	29.71	0.07	0	-	-
3/March	Area	30.82	38.00	12.28	21.34	9.91	2.04	0.08	0.11	0.03
	ArO	26.91	33.18	10.72	18.63	8.66	1.78	0.07	0.09	0.03
4/April	Area	11.03	14.66	10.33	57.84	8.92	11.36	0.21	0.22	0.05
	ArO	9.63	12.80	9.02	50.50	7.79	9.91	0.18	0.19	0.04
5/May	Area	3.74	3.47	1.83	13.56	8.65	22.60	5.80	16.20	38.78
	ArO	3.26	3.03	1.60	11.84	7.55	19.73	5.06	14.14	33.86
6/June	Area	8.18	8.74	4.76	32.26	8.63	29.42	4.09	7.85	10.68
	ArO	7.14	7.63	4.16	28.16	7.54	25.69	3.57	6.86	9.32
7/July	Area	10.45	11.93	8.71	63.28	8.63	10.80	0.31	0.35	0.15
	ArO	9.12	10.41	7.60	55.25	7.54	9.43	0.27	0.31	0.13
8/August	Area	21.15	25.47	14.45	41.71	8.63	2.75	0.16	0.21	0.11
	ArO	18.46	22.24	12.61	36.41	7.54	2.40	0.14	0.18	0.10
9/September	Area	22.48	18.50	9.49	45.13	8.63	9.68	0.31	0.29	0.10
	ArO	19.63	16.15	8.29	39.40	7.56	8.45	0.27	0.25	0.09
10/October	Area	13.06	14.30	7.92	45.80	8.97	21.61	1.14	1.29	0.52
	ArO	11.41	12.48	6.92	39.99	7.83	18.87	0.99	1.13	0.45
11/November	Area	2.67	8.39	7.34	72.30	17.63	6.26	0.03	0.01	-
	ArO	2.33	7.32	6.41	63.12	15.39	5.47	0.03	0.01	-
12/December	Area	-	-	-	-	-	-	-	-	-
	ArO	-	-	-	-	-	-	-	-	-
13/Year	Area	18.63	13.32	8.32	58.42	8.66	6.87	0.13	0.17	0.10
	ArO	16.27	11.63	7.26	51.00	7.56	6.00	0.11	0.15	0.08

Note: Area unit: 10^2 km^2; ArO: Area ratio, unit: %; 4: extremely significant increase; 3: significant increase; 2: slightly significant increase; 1: no significant increase; 0: no change; −1: no significant decrease; −2: slightly significant decrease; −3: significant decrease; −4: extremely significant decrease. 13: represents interannual changes, same as in Figure 9, Table 3, and Figure 10.

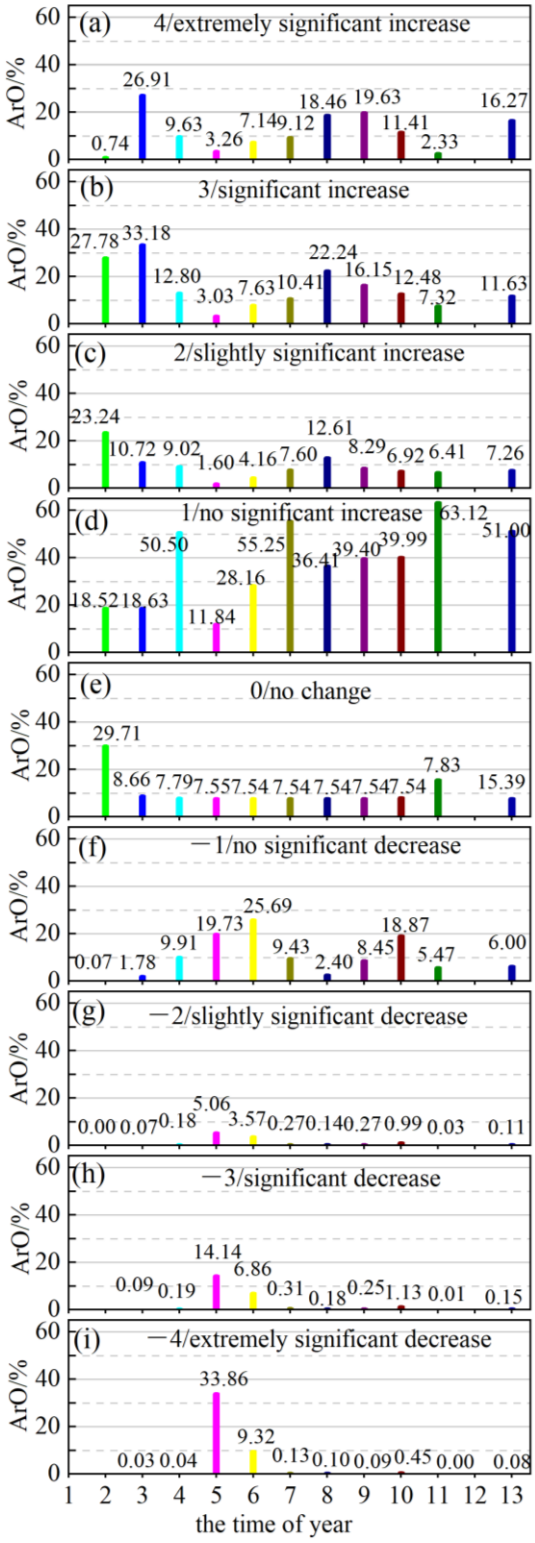

Figure 9. Area ratios of different levels in M–K test for each time period. (**a**) 4 or extremely significant increase; (**b**) 3 or significant increase; (**c**) 2 or slightly significant increase; (**d**) 1 or no significant increase; (**e**) 0 or no change; (**f**) −1 or no significant decrease; (**g**) −2 or slightly significant decrease; (**h**) −3 or significant decrease; (**i**) −4 or extremely significant decrease.

Table 3. Area and proportion of different trends in NPP changes based on the Hurst index from 2001 to 2021.

Time	Parameter	Hurst Index				
		Min-0.25	**0.25–0.50**	**0.50–0.75**	**0.75–1.00**	**Not Included**
1/January	Area	-	-	-	-	-
	ArO	-	-	-	-	-
2/February	Area	0.00	73.75	6.84	0.00	34.04
	ArO	0.00	63.38	5.97	0.00	29.71
3/March	Area	0.01	27.98	76.67	0.05	9.91
	ArO	0.00	24.43	66.94	0.04	8.66
4/April	Area	1.28	98.93	5.48	0.00	8.92
	ArO	1.12	86.37	4.79	0.00	7.79
5/May	Area	0.80	88.79	16.35	0.04	8.65
	ArO	0.69	77.52	14.28	0.03	7.55
6/June	Area	0.15	85.74	20.09	0.00	8.63
	ArO	0.14	74.85	17.54	0.00	7.54
7/July	Area	0.01	94.69	11.28	0.00	8.63
	ArO	0.01	82.67	9.85	0.00	7.54
8/August	Area	6.21	98.29	1.48	0.00	8.63
	ArO	5.42	85.81	1.29	0.00	7.54
9/September	Area	1.29	100.90	3.79	0.00	8.63
	ArO	1.13	88.09	3.31	0.00	7.54
10/October	Area	0.03	53.31	52.22	0.08	8.63
	ArO	0.03	46.55	45.59	0.07	7.83
11/November	Area	1.53	93.86	1.61	0.00	17.63
	ArO	1.33	81.94	1.41	0.00	15.39
12/December	Area	-	-	-	-	-
	ArO	-	-	-	-	-
13/Year	Area	0.05	102.63	3.18	0.01	8.76
	ArO	0.04	89.60	2.77	0.01	7.65

3.4. Future Trend Prediction of NPP Spatiotemporal Changes

In order to better understand the future spatiotemporal trends of NPP in the Hetao Irrigation District of Inner Mongolia, we conducted Hurst index analysis on the monthly and interannual variations of NPP from 2001 to 2021, as shown in Figures 11 and 12. Table 3 provides detailed records of the Hurst index of NPP interannual and monthly changes in terms of the area and area ratio in the study area. In this study, the Hurst index of NPP monthly changes over 21 years ranged from 0.1367 to 0.9035, with the minimum occurring in April (Figure 11d) and the maximum occurring in October (Figure 11j). For the interannual changes of NPP over 21 years, the Hurst index ranged from 0.2112 to 0.782.

Table 3 and Figure 10 below illustrate the area proportions of monthly and annual NPP changes in the Hetao Irrigation District in the future. The monthly results indicate that weak anti-persistence ($0.25 < H \leq 0.5$) dominates in all months except for March. Specifically, the proportion of weak anti-persistence in March is 24.43% (Figure 10b); while weak persistence is highest in March, accounting for 49.03% (Figure 10c). The annual results indicate that the proportions of strong anti-persistence, weak anti-persistence, weak persistence, and strong persistence are 0.04%, 89.60%, 2.77%, and 0.01%, respectively. This suggests that the future trend of NPP in the Hetao Irrigation District exhibits weak anti-persistence, indicating that vegetation NPP may exhibit opposite trends in the future compared to the past. Therefore, without implementing effective measures to improve the ecosystem of the Hetao Irrigation District of Inner Mongolia, there is a trend of decreasing vegetation NPP in the study area.

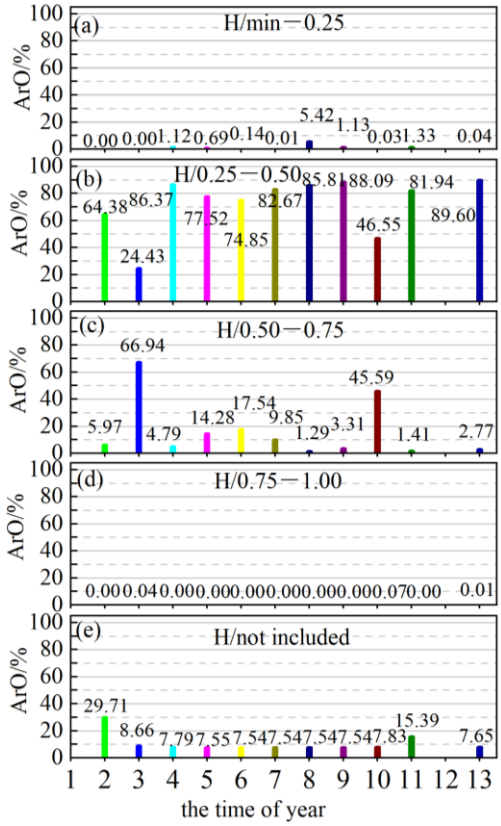

Figure 10. Area ratios of different levels in Hurst index for each time period. (**a**) min–0.25 of Hurst index; (**b**) 0.25–0.50 of Hurst index; (**c**) 0.50–0.75 of Hurst index; (**d**) 0.75–1.00 of Hurst index; (**e**) not included of Hurst index.

It is important to note that the future trends of NPP predicted by the Hurst index do not consider the impact of human activities on NPP. In practice, some human activities can mitigate the negative effects of natural conditions on NPP to some extent. For example, extensive agricultural activities significantly influence carbon absorption and carbon storage in agricultural ecosystems through artificial control of vegetation and soil, such as fertilization, irrigation, and crop rotation systems [54,55]. Land use changes such as afforestation and deforestation also alter the carbon sequestration capacity of ecosystems [56]. Returning straw to the fields can significantly increase organic carbon accumulation and productivity in farmland [57]. Efficient water-saving irrigation significantly improves the productivity and yield of crops in the region [58]. Proper ecological engineering can significantly increase vegetation coverage and aboveground biomass [59]. Furthermore, with the advancement of modern agriculture and smart agriculture, the Chinese government has invested heavily in water conservancy facilities, improvements in irrigation systems, and the development of energy-saving agriculture, which has increased NPP in some regions of China, such as the Lhasa River Basin and the Loess Plateau [60,61]. All these indicate that the transition from NPP reduction to increase can be mitigated or reversed through proactive human activities. Therefore, in response to the national carbon peak policy, it is necessary to formulate relevant measures for the Hetao Irrigation District, such as returning farmland to forests and grasslands, reducing agricultural fertilizers and plastic films, and implementing reasonable irrigation policies, to strengthen ecological environmental governance in the Hetao Irrigation District and improve the environment to enhance vegetation NPP. Previous studies in Inner Mongolia (e.g., [21,28]) also suggest the necessity of taking proactive measures to improve the vegetation NPP in the study area.

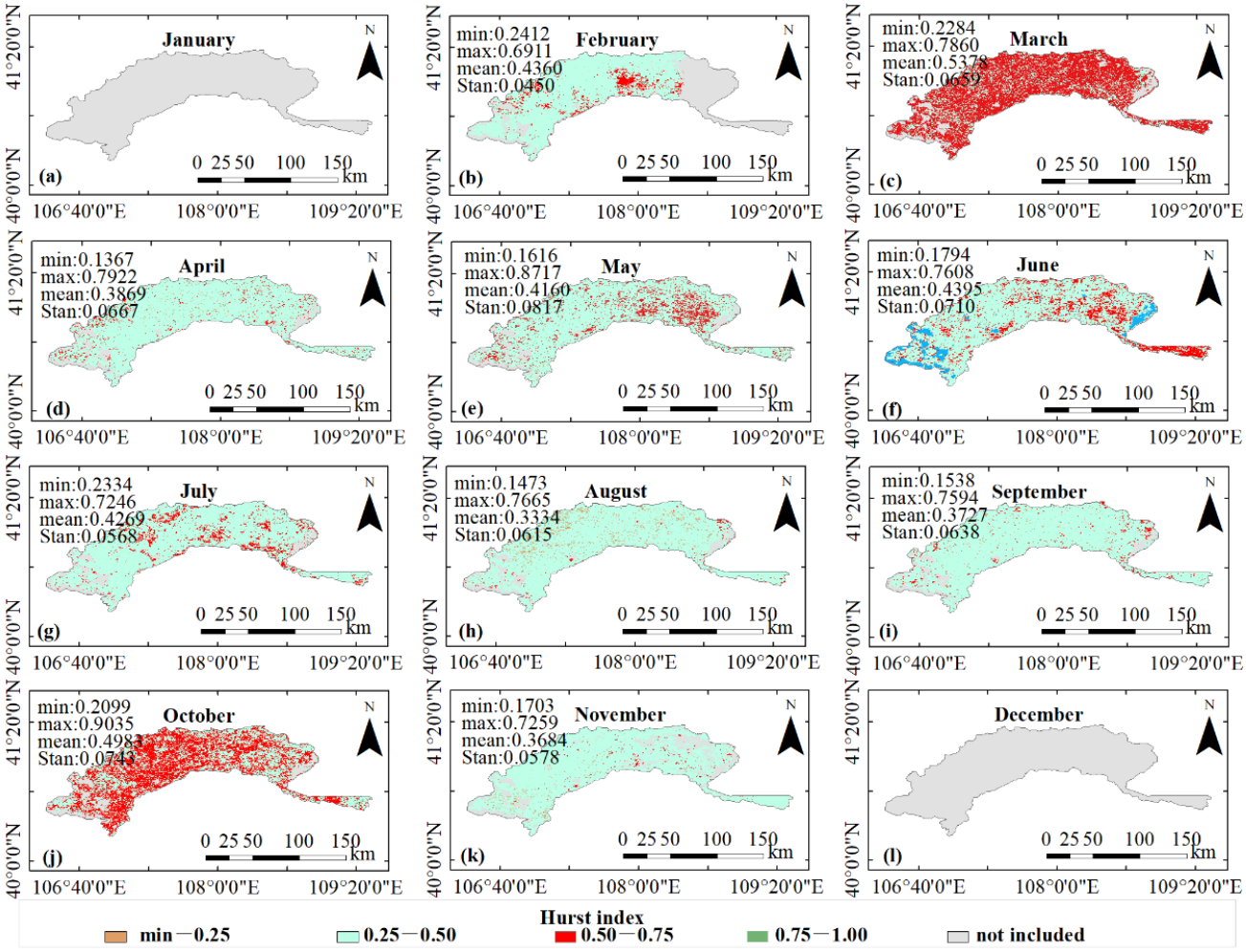

Figure 11. Monthly trend distribution of NPP from 2001 to 2021 based on the Hurst index. (**a**) January; (**b**) February; (**c**) March; (**d**) April; (**e**) May; (**f**) June; (**g**) July; (**h**) August; (**i**) September; (**j**) October; (**k**) November; (**l**) December.

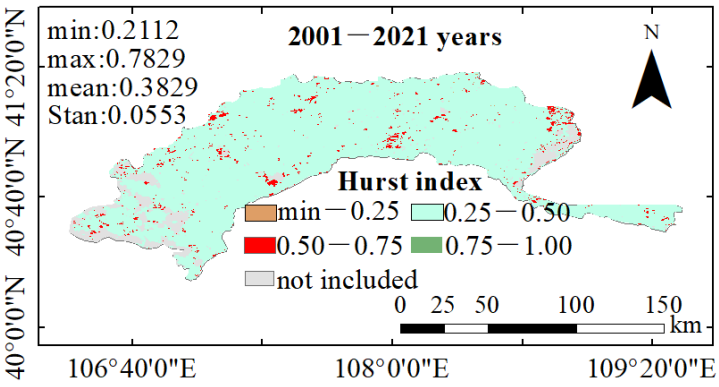

Figure 12. Annual trend distribution of NPP from 2001 to 2021 based on the Hurst index.

4. Conclusions

This study analyzed the spatiotemporal variations in NPP over 21 years in the Hetao Irrigation District in Inner Mongolia and the results are summarized in the following main conclusions: The analysis of time series data revealed that the overall NPP variation in the area over the past 21 years, both on an 8-day and monthly basis, followed an annual cycle, showing an initial increase followed by a decrease in a "∧" shape. The multi-year changes

exhibited an overall fluctuating trend with alternating increases and decreases, showing a slow overall increase. The annual mean NPP ranged between 132.40 and 218.96 $gCm^{-2}a^{-1}$. Significant differences were observed in NPP among different land cover types. Cultivated land emerged as the land cover type with the highest NPP contribution in the Hetao Irrigation District, with the total NPP contribution influenced by the proportional area of different land cover types. The monthly and interannual variations of NPP in the Hetao Irrigation District of Inner Mongolia from 2001 to 2021 have primarily shown no significant increase, with significant decreases and extremely significant decreases observed mainly in May and June. This indicates that over the past 21 years, NPP has not improved, and the Hurst index analysis results predict a decreasing trend in NPP in the study area in the future. These findings underscore the necessity of implementing measures to effectively enhance the carbon sequestration function, thereby achieving the dual goals of high-quality development and ecological environment protection. The results of the study deepen our understanding of the spatiotemporal heterogeneity patterns of NPP in the Hetao Irrigation District of Inner Mongolia. This will assist with the further comprehension of historical changes and future trends of NPP in the study area, providing theoretical support for regional vegetation restoration and ecological rehabilitation efforts.

Author Contributions: Conceptualization, M.P. and C.L.; methodology, M.P.; software, M.P.; validation, M.P. and X.D.; formal analysis, M.P. and C.L.; investigation, P.W.; resources, X.D.; data curation, P.W.; writing—original draft preparation, M.P.; writing—review and editing, M.P.; visualization, X.D.; supervision, C.L.; project administration, C.L.; funding acquisition, M.P. and C.L. All authors have read and agreed to the published version of the manuscript.

Funding: This study was supported by the project ZR2023QC157 supported by Shandong Provincial Natural Science Foundation, the Heze University Doctoral Research Fund (XY21BS24, XY22BS17). We thank the editors and anonymous reviewers for their useful suggestions on improving the quality of this article.

Institutional Review Board Statement: Not applicable.

Informed Consent Statement: Not applicable.

Data Availability Statement: Data are contained within the article.

Conflicts of Interest: The authors declare no conflicts of interest.

References

1. Gang, C.; Zhou, W.; Chen, Y.; Wang, Z.; Sun, Z.; Li, J.; Qi, J.; Odeh, I. Quantitative assessment of the contributions of climate change and human activities on global grassland degradation. *Environ. Earth Sci.* **2014**, *72*, 4273–4282. [CrossRef]
2. Zhang, F.; Hu, X.; Zhang, J.; Li, C.; Zhang, Y.; Li, X. Change in Alpine Grassland NPP in response to climate variation and human activities in the Yellow River Source Zone from 2000 to 2020. *Sustainability* **2022**, *14*, 8790. [CrossRef]
3. Li, Z.; Liu, S.; Tan, Z.; Bliss, N.; Young, C.; West, T.; Ogle, S. Comparing cropland net primary production estimates from inventory, a satellite-based model, and a process-based model in the Midwest of the United States. *Ecol Modell.* **2014**, *277*, 1–12. [CrossRef]
4. Kumar, M.; Singh, R.; Panigrahy, S.; Raghubanshi, A. Carbon density and accumulation in agroecosystem of Indo-Gangetic Plains and Vindhyan highlands. India. *Environ. Monit. Assess.* **2014**, *186*, 4971–4985. [CrossRef] [PubMed]
5. Wang, Y.; Xu, X.; Huang, L.; Yang, G.; Fan, L.; Wei, P.; Chen, G. An improved CASA model for estimating winter wheat yield from remote sensing images. *Remote Sens.* **2019**, *11*, 1088. [CrossRef]
6. Huang, X.; Yang, Y.; Chen, C.; Zhao, H.; Yao, B.; Ma, Z.; Ma, L.; Zhou, H. Quantifying and mapping human appropriation of net Primary productivity in Qinghai Grasslands in China. *Agriculture* **2022**, *12*, 1113. [CrossRef]
7. Koju, U.; Zhang, J.; Maharjan, S.; Bai, Y.; Zhang, S.; Yao, F. Analysis of spatiotemporal dynamics of forest Net Primary Productivity of Nepal during 2000–2015. *Int. J. Remote Sens.* **2020**, *41*, 4336–4364. [CrossRef]
8. Gang, C.; Zhou, W.; Wang, Z.; Chen, Y.; Li, J.; Chen, J.; Qi, J.; Odeh, I.; Groisman, P. Comparative assessment of grassland NPP dynamics in response to climate change in China, North America, Europe and Australia from 1981 to 2010. *Agron. Crop. Sci.* **2015**, *201*, 57–68. [CrossRef]
9. Wang, Y.; Yue, H.; Peng, Q.; He, C.; Hong, S.; Bryan, B. Recent responses of grassland net primary productivity to climatic and anthropogenic factors in Kyrgyzstan. *Land Degrad. Dev.* **2020**, *31*, 2490–2506. [CrossRef]
10. Peng, M.; Han, W.; Li, C.; Li, G.; Yao, X.; Zhang, M. Diurnal and seasonal CO_2 exchange and yield of maize cropland under different irrigation treatments in semiarid Inner Mongolia. *Agric. Water Manag.* **2021**, *255*, 107041. [CrossRef]

11. Li, C.; Han, W.; Peng, M. Improving the spatial and temporal estimating of daytime variation in maize net primary production using unmanned aerial vehicle-based remote sensing. *Int. J. Appl. Earth Obs. Geoinf.* **2021**, *103*, 102467. [CrossRef]
12. Li, C.; Han, W.; Peng, M.; Zhang, F. Abiotic and biotic factors contribute to CO_2 exchange variation at the hourly scale in a semiarid maize cropland. *Sci. Total Environ.* **2021**, *784*, 147170. [CrossRef] [PubMed]
13. Peng, M.; Han, W.; Li, C.; Li, G.; Yao, X.; Shao, G. Modeling the daytime net primary productivity of maize at the canopy scale based on UAV multispectral imagery and machine learning. *J. Clean. Prod.* **2022**, *367*, 133041. [CrossRef]
14. Zhang, Q.; Lei, H.; Yang, D.; Xiong, L.; Liu, P.; Fang, B. Decadal variation in CO_2 fluxes and its budget in a wheat and maize rotation cropland over the North China Plain. *Biogeosciences* **2020**, *17*, 2245–2262. [CrossRef]
15. Dugas, W.; Heuer, M.; Mayeux, H. Carbon dioxide fluxes over bermudagrass, native prairie, and sorghum. *Agric. For. Meteorol.* **1999**, *93*, 121–139. [CrossRef]
16. Yang, F.; He, P.; Ding, H.; Shi, Y. A Monthly High-Resolution Net Primary Productivity Dataset (30 m) of Qinghai Plateau From 1987 to 2021. *IEEE J. Sel. Top. Appl. Earth Observ. Remote Sens.* **2023**, *16*, 8262–8273. [CrossRef]
17. Wang, F.; Wang, F.; Hu, J.; Xie, L.; Yao, X. Rice yield estimation based on an NPP model with a changing harvest index. *IEEE J. Sel. Top. Appl. Earth Obs. Remote Sens.* **2020**, *13*, 2953–2959. [CrossRef]
18. Zhao, J.; Liu, D.; Zhu, Y.; Peng, H.; Xie, H. A review of forest carbon cycle models on spatiotemporal scales. *J. Clean. Prod.* **2022**, *339*, 130692. [CrossRef]
19. Cuo, L.; Zhang, Y.; Xu, R.; Zhou, B. Decadal change and inter-annual variability of net primary productivity on the Tibetan Plateau. *Clim. Dyn.* **2021**, *56*, 1837–1857. [CrossRef]
20. Du, H.; Mao, F.; Zhao, G.; Li, X.; Xu, X.; Ge, H.; Cui, L.; Liu, Y.; Zhu, D.; Li, Y. Estimating and Analyzing the spatiotemporal pattern of aboveground carbon in bamboo forest by combining remote sensing data and improved BIOME-BGC model. *IEEE J. Sel. Top. Appl. Earth Observ. Remote Sens.* **2022**, *11*, 2282–2295. [CrossRef]
21. Zhu, L.; Sun, W.; Wu, J.; Fan, D. Spatiotemporal distribution of carbon sink indicators-NPP and its driving analysis in ordos city, China. *Appl. Sci.* **2023**, *13*, 6457. [CrossRef]
22. Xue, P.; Liu, H.; Zhang, M.; Gong, H.; Cao, L. Nonlinear characteristics of NPP based on ensemble empirical mode decomposition from 1982 to 2015—A case study of six coastal provinces in southeast China. *Remote Sens.* **2021**, *14*, 15. [CrossRef]
23. Yang, H.; Zhong, X.; Deng, S.; Xu, H. Assessment of the impact of LUCC on NPP and its influencing factors in the Yangtze River basin, China. *Catena* **2021**, *206*, 105542. [CrossRef]
24. Cao, Z.; Zhu, T.; Cai, X. Hydro-agro-economic optimization for irrigated farming in an arid region: The Hetao Irrigation District, Inner Mongolia. *Agric. Water Manag.* **2023**, *277*, 108095. [CrossRef]
25. Wan, W.; Lin, Z.; Li, B.; Fang, H.; Wu, H.; Yang, H. Evaluating soil erosion by introducing crop residue cover and anthropogenic disturbance intensity into cropland C-factor calculation: Novel estimations from a cropland-dominant region of Northeast China. *Soil Tillage Res.* **2022**, *219*, 105343. [CrossRef]
26. Hao, L.; Wang, S.; Cui, X.; Zhai, Y. Spatiotemporal dynamics of vegetation net primary productivity and its response to climate change in Inner Mongolia from 2002 to 2019. *Sustainability* **2021**, *13*, 13310. [CrossRef]
27. Li, J.; Cui, Y.; Liu, J.; Shi, W.; Qin, Y. Estimation and analysis of net primary productivity by integrating MODIS remote sensing data with a light use efficiency model. *Ecol. Modell.* **2013**, *252*, 3–10. [CrossRef]
28. Wang, Z.; Zhong, J.; Lan, H.; Wang, Z.; Sha, Z. Association analysis between spatiotemporal variation of net primary productivity and its driving factors in inner mongolia, china during 1994–2013. *Ecol. Indic.* **2019**, *105*, 355–364. [CrossRef]
29. Wang, X.; Wei, Y.; Yang, J. Analysis on water cycling in GSPAC system of Hetao Irrigation District, in Inner Mongolia, China. *J. Irrig. Drain. Eng.* **2004**, *23*, 30–33.
30. Xu, X.; Huang, G.; Qu, Z.; Pereira, L. Assessing the groundwater dynamics and impacts of water saving in the Hetao Irrigation District, Yellow River basin. *Agric. Water Manag.* **2010**, *98*, 301–313. [CrossRef]
31. Son, S.; Wang, M.; Harding, L. Satellite-measured net primary production in the Chesapeake Bay. *Remote Sens. Environ. Mar.* **2014**, *144*, 109–119. [CrossRef]
32. Sen, P. Estimates of the regression coefficient based on Kendall's tau. *J. Am. Stat. Assoc.* **1968**, *63*, 1379–1389. [CrossRef]
33. Theil, H. A rank-invariant method of linear and polynomial regression analysis. *Indag. Math.* **1950**, *12*, 173.
34. Burn, D.; Elnur, M. Detection of hydrologic trends and variability. *J. Hydrodyn.* **2002**, *255*, 107–122. [CrossRef]
35. Zhang, Y.; Gong, J.; Yang, J.; Peng, J. Evaluation of future trends based on the characteristics of net primary production (NPP) changes over 21 years in the Yangtze River Basin in China. *Sustainability* **2023**, *15*, 10606. [CrossRef]
36. Zhang, K.; Kimball, J.; McDonald, K.; Cassano, J.; Running, S. Impacts of large-scale oscillations on pan-Arctic terrestrial net primary production. *Geophys. Res. Lett.* **2007**, *34*, L21403. [CrossRef]
37. Wang, S.; Huang, K.; Yan, H.; Yan, H.; Zhou, L.; Wang, H.; Zhang, J.; Yan, J.; Zhao, L.; Wang, Y.; et al. Improving the light use efficiency model for simulating terrestrial vegetation gross primary production by the inclusion of diffuse radiation across ecosystems in China. *Ecol. Complex.* **2015**, *23*, 1–13. [CrossRef]
38. Xi, M.; Zhang, X.; Kong, F.; Li, Y.; Sui, X.; Wang, X. CO_2 exchange under different vegetation covers in a coastal wetland of Jiaozhou Bay, China. *Ecol. Eng.* **2019**, *137*, 26–33. [CrossRef]
39. Peng, M.; Han, W.; Li, C.; Huang, S. Improving the spatial and temporal estimation of maize daytime net ecosystem carbon exchange variation based on unmanned aerial vehicle multispectral remote sensing. *IEEE J. Sel. Top. Appl. Earth Observ. Remote Sens.* **2021**, *14*, 10560–10570. [CrossRef]

40. Lyapustin, A.; Wang, Y.; Xiong, X.; Meister, G.; Platnick, S. Scientific impact of MODIS C5 calibration degradation and C6 improvement. *Atmos. Meas. Tech.* **2014**, *7*, 4353–4365. [CrossRef]
41. Jahelnabi, A.; Wu, W.; Boloorani, A.; Salem, H.; Nazeer, M.; Fadoul, S.; Khan, M. Assessment the influence of climate and human activities in vegetation degradation using GIS and remote sensing techniques. *Contemp. Probl. Ecol.* **2020**, *13*, 685–693. [CrossRef]
42. Xu, Y.; Lu, Y.; Zou, B.; Xu, M.; Feng, Y. Unraveling the enigma of NPP variation in Chinese vegetation ecosystems: The interplay of climate change and land use change. *Sci. Total Environ.* **2024**, *912*, 169023. [CrossRef] [PubMed]
43. Wang, W.; Wang, J.; Liu, X.; Zhou, G.; Yan, J. Decadal drought deaccelerated the increasing trend of annual net primary production in tropical or subtropical forests in southern China. *Sci. Rep.* **2016**, *6*, 28640. [CrossRef] [PubMed]
44. Zhang, W.; Chen, S.; Chen, J.; Wei, L.; Han, X.; Lin, G. Biophysical regulations of carbon fluxes of a steppe and a cultivated cropland in semiarid Inner Mongolia. *Agric. For. Meteorol.* **2007**, *146*, 216–229. [CrossRef]
45. Zhang, T.; Peng, J.; Liang, W.; Yang, Y.; Liu, Y. Spatial-temporal patterns of water use efficiency and climate controls in China's loess plateau during 2000–2010. *Sci. Total Environ.* **2016**, *565*, 105–122. [CrossRef] [PubMed]
46. Liu, Y.; Xiao, J.; Ju, W.; Zhou, Y.; Wang, S.; Wu, X. Water use efficiency of China's terrestrial ecosystems and responses to drought. *Sci. Rep.* **2015**, *5*, 13799. [CrossRef]
47. Lu, X.; Zhuang, Q. Evaluating evapotranspiration and water-use efficiency of terrestrial ecosystems in the conterminous United States using MODIS and AmeriFlux data. *Remote Sens. Environ.* **2010**, *114*, 1924–1939. [CrossRef]
48. Zhao, M.; Running, S. Drought-induced reduction in global terrestrial net primary production from 2000 through 2009. *Science* **2010**, *329*, 940–943. [CrossRef]
49. Li, Z.; Zhang, R.; Wang, X.; Chen, F.; Tian, C. Growing season carbon dioxide exchange in flooded non-mulching and non-flooded mulching cotton. *PLoS ONE* **2012**, *7*, e50760. [CrossRef]
50. Li, G.; Cui, J.; Han, W.; Zhang, H.; Huang, S.; Chen, H.; Ao, J. Crop type mapping using time-series Sentinel-2 imagery and U-Net in early growth periods in the Hetao irrigation district in China. *Comput. Electron. Agric.* **2022**, *203*, 107478. [CrossRef]
51. Valerie, A.; Cook, F.J. Relationships between soil respiration and soil moisture. *Soil Biol. Biochem.* **2008**, *40*, 1013–1018.
52. Wu, J.; Zhang, Q.; Li, A.; Liang, C. Historical landscape dynamics of Inner Mongolia: Patterns, drivers, and impacts. *Landsc. Ecol.* **2015**, *30*, 1579–1598. [CrossRef]
53. Gao, L.; Kinnucan, H.; Zhang, Y.; Qiao, G. The effects of a subsidy for grassland protection on livestock numbers, grazing intensity, and herders' income in Inner Mongolia. *Land Use Policy* **2016**, *54*, 302–312. [CrossRef]
54. Huang, K.; Xia, J.; Wang, Y.; Ahlström, A.; Chen, J.; Cook, R.B.; Cui, E.; Fang, Y.; Fisher, J.B.; Huntzinger, D.N. Enhanced peak growth of global vegetation and its key mechanisms. *Nat. Ecol. Evol.* **2018**, *2*, 1897–1905. [CrossRef] [PubMed]
55. Xie, W.; Zhu, A.; Ali, T.; Zhang, Z.; Chen, X.; Wu, F.; Huang, J.; Davis, K. Crop switching can enhance environmental sustainability and farmer incomes in China. *Nature* **2023**, *616*, 300–305. [CrossRef]
56. Xiao, J. Satellite evidence for significant biophysical consequences of the "Grain for Green" Program on the Loess Plateau in China. J. *Geophys. Res. Biogeosci.* **2014**, *119*, 2261–2275. [CrossRef]
57. Hao, X.; He, W.; Lam, S.; Li, P.; Zong, Y.; Zhang, D.; Li, F. Enhancement of no-tillage, crop straw return and manure application on field organic matter content overweigh the adverse effects of climate change in the arid and semi-arid Northwest China. *Agric. For. Meteorol.* **2020**, *295*, 1–10. [CrossRef]
58. Li, R.; Shi, H.; Flerchinger, G.; Akae, T. Simulation of freezing and thawing soils in Inner Mongolia Hetao Irrigation District, China. *Geoderma* **2012**, *173*, 28–33. [CrossRef]
59. Niu, Q.; Xiao, X.; Zhang, Y.; Qin, Y.; Dang, X.; Wang, J.; Zou, Z.; Doughty, R.B.; Brandt, M.; Tong, X.; et al. Ecological engineering projects increased vegetation cover, production, and biomass in semiarid and subhumid Northern China. *Land Degrad. Dev.* **2019**, *30*, 1620–1631. [CrossRef]
60. Li, D.; Luo, H.; Hu, T.; Shao, D.; Cui, Y.; Khan, S.; Luo, Y. Identification of the roles of climate factors, engineering construction, and agricultural practices in vegetation dynamics in the Lhasa River Basin, Tibetan Plateau. *Remote Sens.* **2020**, *12*, 883. [CrossRef]
61. Li, Y.; Zhang, X.; Cao, Z.; Liu, Z.; Lu, Z.; Liu, Y. Towards the progress of ecological restoration and economic development in China's Loess Plateau and strategy for more sustainable development. *Sci. Total Environ.* **2021**, *756*, 143676.